Applied Physics Letters ARTICLE pubs.aip.org/aip/apl

Transmission diffuse EUV scattering by nanoscale Lamb waves in thin membranes

Cite as: Appl. Phys. Lett. **129**, 062201 (2026); doi: 10.1063/5.0343558
Submitted: 13 May 2026 · Accepted: 25 July 2026 ·
Published Online: 10 August 2026

Alessandra Milloch,[1,a)] Naman Agarwal,[1] Jörn Bonse,[2] Nicolas Jaouen,[3] Emanuele Pedersoli,[1] Luca Sbuelz,[4] Klaus Sokolowski-Tinten,[5] Roberta Totani,[1] Sergei Urazhdin,[6] Adriana Valerio,[1] Alexei A. Maznev,[7] Filippo Bencivenga,[1] and Flavio Capotondi[1]

AFFILIATIONS

[1]Elettra - Sincrotrone Trieste S.C.p.A., Trieste, Italy
[2]Bundesanstalt für Materialforschung und -prüfung (BAM), Unter den Eichen 87, 12205 Berlin, Germany
[3]Synchrotron SOLEIL, L'Orme des Merisiers, 91190 Saint-Aubin, France
[4]CNR-Consiglio Nazionale Delle Ricerche, Istituto Officina Dei Materiali, Area Science Park, Strada Statale 14 Km 163.5, Basovizza, Trieste 34149, Italy
[5]Faculty of Physics and Center for Nanointegration Duisburg-Essen (CENIDE), University of Duisburg-Essen, Lotharstrasse 1, 47048 Duisburg, Germany
[6]Department of Physics, Emory University, Atlanta, Georgia 30322, USA
[7]Department of Chemistry, Massachusetts Institute of Technology, Cambridge, Massachusetts 02139, USA

[a)]Author to whom correspondence should be addressed: alessandra.milloch@elettra.eu

ABSTRACT

We report time-resolved diffuse extreme ultraviolet (EUV) scattering measurements of optically excited acoustic waves in thin Ti/SiN bilayers in transmission geometry. Following femtosecond optical excitation, the EUV diffuse scattering signal yields circular fringe patterns evolving as a function of the time delay between the optical pump and EUV probe pulses. We demonstrate that these patterns originate from multiple guided acoustic modes (Lamb waves) with wavelengths in the range 60–400 nm. By comparing the experimental frequency–wavevector maps with calculated dispersion curves, we show that diffuse scattering signal from Lamb waves is enhanced at discrete frequencies corresponding to longitudinal thickness resonances of the membrane. This observation indicates that Lamb waves with high in-plane wavevectors originate from the scattering of longitudinal thickness resonances by surface roughness. Our findings establish time-resolved diffuse EUV scattering as an efficient tool for probing nanoscale Lamb waves, applicable to the characterization of elastic properties of thin membranes.

Measurements of guided acoustic waves at the nanoscale are of broad scientific and technological interest, yet pose formidable experimental challenges.[1,2] The wavevector range accessible with traditional optical methods, such as Brillouin light scattering[3] and laser-induced transient gratings (TG),[4,5] is limited by twice the optical wavevector. In recent years, the extension of the TG technique into the extreme ultraviolet (EUV) range[6,7] enabled excitation and probing of surface acoustic waves (SAWs) in bulk samples[8] and Lamb waves in thin membranes[9,10] with wavelengths down to tens of nanometers. However, EUV TG measurements require a complicated setup[11,12] and can probe only a single wavevector at a time.

More recently, a free electron laser approach based on diffuse EUV scattering (DES) was shown to enable time-resolved observation of nanoscale SAWs with wavelengths from tens to hundreds of nanometers, generated by uniform femtosecond optical excitation in a wide range of metal and semiconductor samples.[13] The DES method offers a high-wavevector surface phonon spectroscopy tool with a much simpler setup than EUV TG[13] and is capable of probing a broad range of acoustic wavevectors in a single measurement. So far, DES experiments have been performed exclusively in reflection geometry,[13] making the technique primarily sensitive to surface displacements. Furthermore, the physical mechanism responsible for the optical generation of the high-wavevector acoustic modes detected by DES has not been conclusively clarified. Previous work showed that the optical excitation of nanoscale SAWs is facilitated by surface roughness, found even in very smooth samples.[13] Two possible mechanisms have been proposed:[13] (i) thermoelastic excitation of longitudinal acoustic waves propagating normally to the sample surface,[14] followed by their scattering into laterally propagating modes by surface roughness,[15] akin to bulk-to-surface mode conversion mediated by a grating fabricated on the sample surface;[16] and (ii) inhomogeneous optical absorption resulting from light scattering at a rough surface,[17] which produces spatially varying thermal stresses and directly launches SAWs with finite wavevectors. While Ref. 13 suggested that the former mechanism was more likely, direct experimental evidence supporting this hypothesis was lacking.

In this report, we demonstrate transmission-mode DES measurements on free-standing bilayer Ti/SiN membranes. The frequency–wavevector maps constructed from the experimental data reveal a number of Lamb modes (i.e., guided acoustic waves propagating in thin plates) in the wavevector range 0.015–0.11 nm^{-1}, with maxima at nearly harmonic discrete frequencies. Our calculations show that these frequencies correspond to longitudinal thickness resonances of the membranes, providing strong support for the mechanism based on the scattering of zero in-plane wavevector longitudinal modes into Lamb waves.

The experimental principle of DES is illustrated in Fig. 1(a). After optical excitation with an ultrashort laser pulse, the scattering from a time-delayed EUV pulse from a free electron laser (FEL) forms a time-dependent circular fringe pattern, which is recorded by a two-dimensional CCD detector as a function of the optical pump-FEL

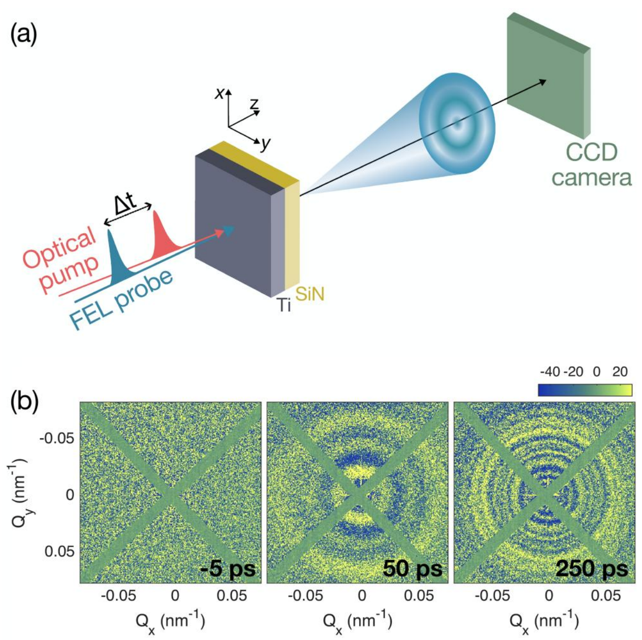

FIG. 1. (a) Sketch of the time-resolved DES experimental setup in transmission geometry. (b) Differential DES signal measured in transmission geometry for a 200-nm-Ti/200-nm-SiN sample at selected time delays Δt after optical excitation (color scale: counts per pixel).

probe time delay Δt. At each point of the detector, the signal exhibits temporal oscillations at the frequency of the acoustic wave corresponding to the wavevector determined by the scattering geometry. The detection of this coherent oscillatory signal relies on a heterodyne interference mechanism between the static scattering from the surface roughness and the time-dependent scattering from the generated acoustic waves. Because the excitation of acoustic waves at a given wavevector is mediated by the corresponding spatial Fourier component of the surface roughness, the resulting acoustic displacement inherits the same spatial phase, and the two scattered fields are phase locked, enabling coherent detection of acoustic waves even for an arbitrary roughness distribution.[13] The measurements were performed at the DiProI end station at the FERMI FEL facility.[18,19] Optical excitation was provided by a laser pump pulse with a wavelength of 790 nm and 80 fs time duration; the phonon dynamics were probed by an FEL pulse with a wavelength of 17.8 nm and 50 fs time duration. Pump and probe pulses impinge onto the sample at nearly normal incidence, with a 2° offset between them, and are focused to $300 \times 250\ \mu\text{m}^2$ and $150 \times 120\ \mu\text{m}^2$ FWHM spot sizes, respectively. The laser fluence was 17 mJ/cm^2, the FEL fluence was 2 mJ/cm^2. Both the laser and FEL fluences were below the multi-shot threshold of any permanent surface modification. This enables signal accumulation over many identical pump–probe irradiation events at the same sample location. The samples consisted of thin titanium films with thicknesses ranging from 70 to 200 nm, deposited on free-standing SiN membranes of 100 or 200 nm thickness. The transmitted FEL radiation was recorded by a CCD detector positioned at a distance between 46 and 60 mm from the interaction point, depending on the measurement, with a beam stop used to block the direct beam. The pump–probe time delay Δt was scanned from −5 ps to 1 ns, sampled in 5 ps steps. At each time delay, the detector was exposed to 1500 FEL shots at a repetition rate of 50 Hz. To characterize the background, three additional reference images were acquired every 10 time points: with only the EUV probe beam, with only the optical pump beam, and with no radiation in the chamber. These measurements allowed the characterization of the static scattering from the unexcited sample, the contribution of optical stray light, and the dark signal of the CCD detector, respectively. The DES signal is then obtained from the CCD images after background subtraction and coordinate transformation, following the procedure detailed in supplementary material Sec. S1. The resulting differential (pump on – pump off) DES patterns are shown in Fig. 1(b) for selected time delays. The horizontal and vertical axes represent the components Q_x and Q_y of the scattering wavevector. The X-shaped feature visible in Fig. 1(b) is due to the beam blocker. For $\Delta t < 0$, the signal image is featureless, whereas after the excitation by the pump pulse, a characteristic time-dependent ring pattern is detected, with the fringes becoming denser with increasing delay. A movie showing the full time evolution, up to 1 ns, of this fringe pattern is available in the supplementary material. Owing to the isotropy of the system in the (Q_x, Q_y) plane, the DES signal can be azimuthally integrated over concentric circles.[13] A Fourier transform of the time-domain data then yields the frequency–wavevector map that reveals the dependence of the oscillation frequency on Q, i.e., the acoustic wave dispersion.[13]

We first consider a 200-nm-Ti/200-nm-SiN sample. Figure 2(a) shows the dependence of the DES signal on the in-plane wavevector magnitude Q and the pump–probe delay Δt, obtained by azimuthal

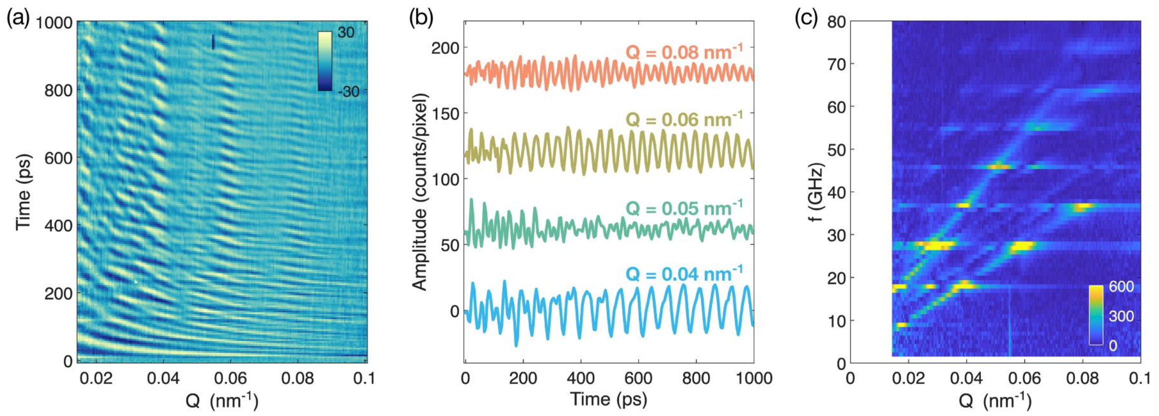

FIG. 2. (a) Azimuthally integrated DES intensity as a function of wavevector Q and pump–probe delay Δt, measured in transmission geometry for the 200-nm-Ti/200-nm-SiN sample (color scale: counts per pixel). (b) Time dependence of the DES signal in (a) at selected Q values. (c) Modulus of the temporal Fourier transform of the data in (a), yielding a frequency–wavevector map (color scale: arbitrary units).

integration of the signal images. Clear temporal oscillations are observed [see time traces at selected wavevectors in Fig. 2(b)]. A temporal Fourier transform of the time-domain data in Fig. 2(a) results in the frequency–wavevector map of Fig. 2(c). Two main features can be identified: (i) multiple dispersive branches corresponding to different acoustic modes and (ii) bright spots appearing at discrete nearly harmonic frequencies. To interpret these observations and clarify the nature of the bright spots, we calculate the acoustic dispersion relations of a free-standing bilayer structure and compare them with the experimental data.

The acoustic modes are obtained by solving the elastic wave equation for an isotropic medium, given by[20]

$$c_{44}\nabla^2\boldsymbol{v} + (c_{11} - c_{44})\nabla(\nabla\cdot\boldsymbol{v}) = \rho\frac{\partial^2\boldsymbol{v}}{\partial t^2}, \tag{1}$$

where $\boldsymbol{v}$ is the velocity field, ρ is the mass density, and c_{11} and c_{44} are the elastic moduli, related to the longitudinal and shear sound velocities as $v_l = \sqrt{c_{11}/\rho}$ and $v_s = \sqrt{c_{44}/\rho}$, respectively. We seek solutions to Eq. (1) for waves with displacements in the sagittal plane by expressing the displacement field in each layer as a superposition of partial longitudinal and transverse waves at a given in-plane wavevector.[4,21] The dispersion relation $f(Q)$ and the displacement profiles of the acoustic eigenmodes supported by the free-standing bilayer are then determined by imposing appropriate boundary conditions, namely, zero stress at the free surfaces and continuity of stress and velocity at the interface between the two layers. These modes correspond to guided acoustic excitations, commonly referred to as Lamb waves, involving coupled longitudinal and shear displacements.[4,22]

In Fig. 3, the calculated dispersion curves for a 200-nm-Ti/200-nm-SiN bilayer are overlaid on the experimental frequency–wavevector map [same data as in Fig. 2(c), shown here on a logarithmic color scale]. The model uses $v_l = 6000$ m/s, $v_s = 3175$ m/s, and $\rho = 4.5$ g/cm^3 for Ti, and $v_l = 9600$ m/s, $v_s = 5400$ m/s, and $\rho = 3.1$ g/cm^3 for SiN. The chosen acoustic velocities, remaining within the range of sound velocity values reported in the literature[10,23–27] and consistent with expected variations of thin-film properties depending on the deposition conditions, yield good agreement between experiment and theory. The lowest-frequency branch (thicker white line in Fig. 3) corresponds to a Rayleigh-like mode localized at the Ti surface, similar to what would be predominantly detected in reflection geometry. A number of higher-frequency Lamb modes are also detected. The displacement fields of these modes extend across the film thickness, rather than being confined to the surface. These

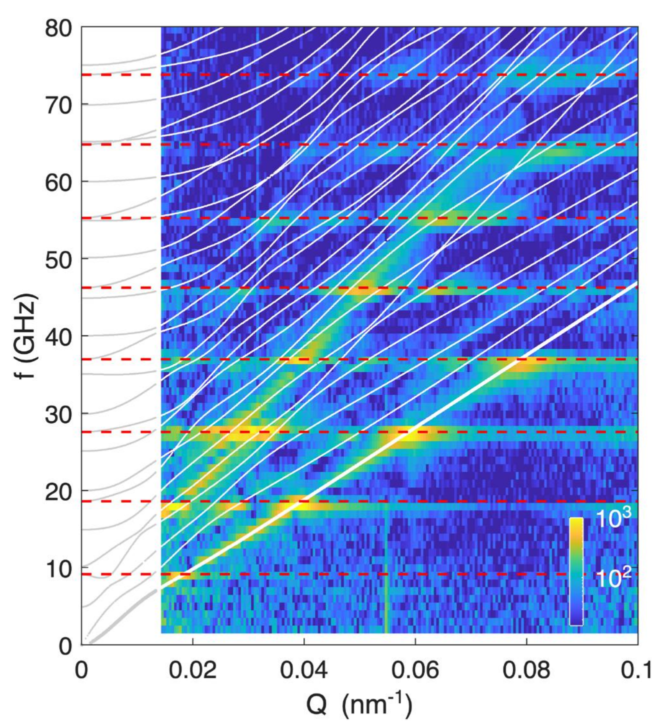

FIG. 3. Frequency–wavevector experimental map from Fig. 2(c) shown on a logarithmic color scale and overlaid with the calculated dispersion curves (white lines) of acoustic modes in the 200-nm-Ti/200-nm-SiN bilayer. The red dashed lines indicate the frequencies of the zero-in-plane wavevector ($Q = 0$) purely longitudinal modes.

observations establish that DES in transmission geometry provides access to both surface-localized waves and guided Lamb modes, over a broad acoustic wavevector range corresponding to wavelengths between 60 and 400 nm.

In addition to the continuous dispersive branches, bright spots are observed at the intersections of the Lamb wave dispersion curves with discrete frequencies. We find that these are the frequencies of the zero in-plane wavevector ($Q = 0$) longitudinal modes, i.e., longitudinal thickness resonances with displacement perpendicular to the surface.[28] At $Q = 0$, the modes are separated into purely longitudinal and purely transverse; the resonance frequencies of the longitudinal ones are indicated by red dashed lines in Fig. 3. These modes are well known to be generated by pulsed laser excitation of thin plates and membranes.[29] The absorption of the pump pulse at the Ti surface (the absorption length in Ti at the optical pump wavelength is ~15 nm) and subsequent rapid thermal expansion launches a longitudinal acoustic pulse propagating normally to the surface. Subsequent multiple reflections from the surfaces and the Ti/SiN interface produce an acoustic field that can be represented as a superposition of the longitudinal thickness resonance modes. These modes cannot contribute to diffuse EUV scattering directly, as their displacement patterns are uniform in the *xy* plane. However, in the presence of surface roughness, they will undergo scattering into Lamb modes with non-zero Q, just as longitudinal waves incident on a surface of a semi-infinite solid are partially scattered into surface Rayleigh waves.[15] The multiple reflections of the longitudinal resonance modes from the membrane surfaces then lead to periodic excitation of Lamb modes. This model explains why we observe an enhanced DES signal for the Lamb modes at the intersections of their dispersion curves with the longitudinal thickness resonance frequencies. This mechanism is also reflected in the time-domain waveforms [see Fig. 2(b)], where the resonance-enhanced modes do not exhibit a simple exponential decay within the experimental time window (for this reason, a direct determination of the intrinsic attenuation time of the Lamb modes is not straightforward).

To further validate our interpretation, we performed DES measurements on thinner Ti/SiN samples, with Ti layer thicknesses of 70 and 100 nm deposited on 100-nm-thick free-standing SiN membranes. The time-domain DES data are reported in the supplementary material (Fig. S1), while Fig. 4 displays the corresponding Fourier-transformed frequency–wavevector maps. We note that the DES signal intensity is larger for the 100 nm sample than for the 70 nm sample, consistent with its higher surface roughness (3.3 nm, compared to 2.3 nm for the 70 nm sample; see Figs. S4 and S5 in the supplementary material) and with the roughness-mediated generation of Lamb modes. In these thinner samples, the reduced number of modes in the frequency–wavevector maps, compared to the 200-nm sample, facilitates the comparison between experiment and calculated dispersion curves. The dispersion relations were calculated by selecting longitudinal and shear sound velocities within literature ranges and tuning the effective Ti layer thickness to match the data. The best match is found for effective Ti thicknesses of 97 and 71 nm for the two samples, in good agreement with the expected thickness values. The sound velocities are set, for both samples, to $v_l = 6050$ m/s and $v_s = 3175$ m/s for Ti and $v_l = 9800$ m/s and $v_s = 6000$ m/s for SiN; the slight deviations in the sound velocities relative to the 200-nm-Ti/200-nm-SiN sample (Fig. 3), most pronounced for the SiN layer, can

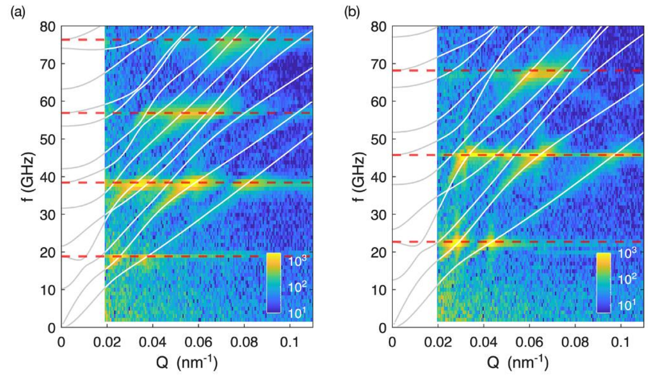

FIG. 4. DES frequency–wavevector maps for Ti/SiN samples with Ti layers of nominal thicknesses of 100 (a) and 70 nm (b). Calculated dispersion relations for the corresponding Ti/SiN bilayers are overlaid as white solid lines. The red dashed lines indicate the resonance frequencies of purely longitudinal thickness modes at $Q = 0$.

be attributed to the different manufacturers of the SiN membranes used in the two sample batches. The resulting calculated dispersion curves (white solid lines in Fig. 4) reproduce well the continuous dispersive branches as well as the bright spots observed at the longitudinal thickness resonance frequencies (red dashed lines), confirming the interpretation discussed above.

Representative displacement-field patterns for modes in the 70 nm sample are shown in supplementary material Fig. S2 and confirm that the modes detected in transmission geometry include both surface-localized waves and guided modes with displacement extending across the membrane thickness. The strongest signal is associated with modes exhibiting large displacement in the Ti layer. This suggests that scattering of longitudinal thickness resonances into Lamb waves occurs predominantly at the Ti surface, consistent with x-ray reflectivity and atomic force microscope measurements indicating significantly higher roughness of the Ti surface compared to the SiN layer (see supplementary material Figs. S5 and S6). We note that the experimentally observed mode intensity depends not only on the amplitude with which a given Lamb mode is generated but also on its detection efficiency in DES. The latter can be estimated from the depth-integrated refractive-index modulation associated with the density modulation of each mode, calculated from the corresponding displacement profiles. This analysis indicates that modes whose dispersion approaches the Rayleigh-wave and longitudinal sound velocities of the Ti layer are expected to generate the strongest scattered signal (see Fig. S3 in the supplementary material), in qualitative agreement with the experimentally observed frequency–wavevector maps.

In conclusion, we observed dynamic ring patterns in diffuse EUV scattering in transmission geometry from bilayer Ti/SiN membranes following femtosecond optical excitation. We found that the experimental signal originates from Lamb waves in the wavevector range ~0.015–0.1 nm^{-1}, which corresponds to 60–400 nm wavelengths. The Lamb waves are preferably excited at discrete frequencies corresponding to longitudinal thickness resonances of the membranes. Together with the results of Ref. 13, our observations support the mechanism in which nanoscale acoustic modes are produced by scattering of longitudinal thickness resonances by surface roughness.

We believe that the reported phenomenon is universal and will be observed on any sample thin enough to transmit the EUV probe beam and absorbing optical pump light. Transmission-mode diffuse EUV scattering offers a spectroscopy tool for studying nanoscale Lamb waves and for mechanical characterization of free-standing membranes. The extension to multilayer and nano-patterned structures and materials with anisotropic elastic properties will further broaden the applications of this approach. In addition, studying the scattering of thickness resonances into Lamb waves will help understand the role of surface roughness in limiting the Q-factor of thin-film acoustic resonators used in telecommunication devices as their frequency is pushed into the tens of GHz range.[30] Furthermore, the presence of a tangible acoustic response has to be taken into account while interpreting time-resolved EUV diffuse scattering measurements, for example, from magnetic textures.[31–33] Finally, we expect that the time-resolved DES technique can be implemented using table-top high-harmonic generation sources, which will enhance its accessibility and enable wider adoption beyond FEL facilities.

See the supplementary material for details of the data processing procedure, additional diffuse scattering data and Lamb wave calculations, AFM and x-ray reflectivity characterization, and a supplementary movie showing the time evolution of the diffuse scattering signal images.

K.S.T. acknowledges support by the Deutsche Forschungsgemeinschaft (DFG, German Research Foundation) through Project No. 278162697-SFB 1242. S.U. acknowledges financial support from the U.S. National Science Foundation Award No. ECCS-2448290. A.A.M. acknowledges support from the MIT School of Science Sloan Fund.

AUTHOR DECLARATIONS

Conflict of Interest

The authors have no conflicts to disclose.

Author Contributions

Alessandra Milloch: Data curation (lead); Formal analysis (lead); Investigation (equal); Methodology (equal); Software (equal); Visualization (equal); Writing – original draft (lead); Writing – review & editing (lead). **Naman Agarwal:** Investigation (equal); Methodology (equal); Writing – review & editing (equal). **Jörn Bonse:** Investigation (equal); Validation (equal); Writing – review & editing (equal). **Nicolas Jaouen:** Investigation (equal); Validation (equal); Writing – review & editing (equal). **Emanuele Pedersoli:** Data curation (equal); Investigation (equal); Methodology (equal); Software (equal); Writing – review & editing (equal). **Luca Sbuelz:** Data curation (equal); Investigation (equal); Methodology (equal). **Klaus Sokolowski-Tinten:** Investigation (equal); Validation (equal); Writing – review & editing (equal). **Roberta Totani:** Data curation (equal); Investigation (equal); Methodology (equal). **Sergei Urazhdin:** Investigation (equal); Methodology (equal); Validation (equal); Writing – review & editing (equal). **Adriana Valerio:** Investigation (equal); Methodology (equal); Writing – review & editing (equal). **Alexei A. Maznev:** Conceptualization (equal); Data curation (equal); Formal analysis (equal); Supervision (equal); Validation (equal); Writing – review & editing (equal). **Filippo Bencivenga:** Conceptualization (equal); Data curation (equal); Formal analysis (equal); Investigation (equal); Supervision (equal); Writing – review & editing (equal). **Flavio Capotondi:** Conceptualization (equal); Data curation (equal); Formal analysis (equal); Investigation (equal); Methodology (equal); Project administration (equal); Resources (equal); Software (equal); Supervision (equal); Validation (equal); Visualization (equal); Writing – review & editing (equal).

DATA AVAILABILITY

The data that support the findings of this study are available from the corresponding author upon reasonable request.

REFERENCES

[1]P. Delsing, A. N. Cleland, M. J. A. Schuetz, J. Knörzer, G. Giedke, J. I. Cirac, K. Srinivasan, M. Wu, K. C. Balram, C. Bäuerle, T. Meunier, C. J. B. Ford, P. V. Santos, E. Cerda-Méndez, H. Wang, H. J. Krenner, E. D. S. Nysten, M. Weiß, G. R. Nash, L. Thevenard, C. Gourdon, P. Rovillain, M. Marangolo, J.-Y. Duquesne, G. Fischerauer, W. Ruile, A. Reiner, B. Paschke, D. Denysenko, D. Volkmer, A. Wixforth, H. Bruus, M. Wiklund, J. Reboud, J. M. Cooper, Y. Fu, M. S. Brugger, F. Rehfeldt, and C. Westerhausen, "The 2019 surface acoustic waves roadmap," J. Phys. D: Appl. Phys. **52**, 353001 (2019).
[2]R. C. Ng, A. El Sachat, F. Cespedes, M. Poblet, G. Madiot, J. Jaramillo-Fernandez, O. Florez, P. Xiao, M. Sledzinska, C. M. Sotomayor-Torres, and E. Chavez-Angel, "Excitation and detection of acoustic phonons in nanoscale systems," Nanoscale **14**, 13428 (2022).
[3]M. Grimsditch, R. Bhadra, and I. K. Schuller, "Lamb waves in unsupported thin films: A Brillouin-scattering study," Phys. Rev. Lett. **58**, 1216 (1987).
[4]A. R. Duggal, J. A. Rogers, and K. A. Nelson, "Real-time optical characterization of surface acoustic modes of polyimide thin-film coatings," J. Appl. Phys. **72**, 2823 (1992).
[5]J. A. Rogers, A. A. Maznev, M. J. Banet, and K. A. Nelson, "Optical generation and characterization of acoustic waves in thin films: Fundamentals and applications," Annu. Rev. Mater. Sci. **30**, 117 (2000).
[6]L. Foglia, R. Mincigrucci, A. Maznev, G. Baldi, F. Capotondi, F. Caporaletti, R. Comin, D. De Angelis, R. Duncan, D. Fainozzi, G. Kurdi, J. Li, A. Martinelli, C. Masciovecchio, G. Monaco, A. Milloch, K. Nelson, C. Occhialini, M. Pancaldi, E. Pedersoli, J. Pelli-Cresi, A. Simoncig, F. Travasso, B. Wehinger, M. Zanatta, and F. Bencivenga, "Extreme ultraviolet transient gratings: A tool for nanoscale photoacoustics," Photoacoustics **29**, 100453 (2023).
[7]F. Bencivenga, F. Capotondi, L. Foglia, R. Mincigrucci, and C. Masciovecchio, "Extreme ultraviolet transient gratings," Adv. Phys.: X **8**, 2220363 (2023).
[8]A. A. Maznev, R. Mincigrucci, F. Bencivenga, V. Unikandanunni, F. Capotondi, G. Chen, Z. Ding, R. A. Duncan, L. Foglia, M. G. Izzo, C. Masciovecchio, A. Martinelli, G. Monaco, E. Pedersoli, S. Bonetti, and K. A. Nelson, "Generation and detection of 50 GHz surface acoustic waves by extreme ultraviolet pulses," Appl. Phys. Lett. **119**, 044102 (2021).
[9]D. Naumenko, R. Mincigrucci, M. Altissimo, L. Foglia, A. Gessini, G. Kurdi, I. Nikolov, E. Pedersoli, E. Principi, A. Simoncig, M. Kiskinova, C. Masciovecchio, F. Capotondi, and F. Bencivenga, "Thermoelasticity of nanoscale silicon carbide membranes excited by extreme ultraviolet transient gratings: implications for mechanical and thermal management," ACS Appl. Nano Mater. **2**, 5132 (2019).
[10]A. Milloch, R. Mincigrucci, F. Capotondi, D. De Angelis, L. Foglia, G. Kurdi, D. Naumenko, E. Pedersoli, J. S. Pelli-Cresi, A. Simoncig, B. Wehinger, C. Masciovecchio, and F. Bencivenga, "Nanoscale thermoelasticity in silicon nitride membranes: Implications for thermal management," ACS Appl. Nano Mater. **4**, 10519 (2021).
[11]R. Mincigrucci, L. Foglia, D. Naumenko, E. Pedersoli, A. Simoncig, R. Cucini, A. Gessini, M. Kiskinova, G. Kurdi, N. Mahne, M. Manfredda, I. Nikolov, E. Principi, L. Raimondi, M. Zangrando, C. Masciovecchio, F. Capotondi, and F. Bencivenga, "Advances in instrumentation for FEL-based four-wave-mixing experiments," Nucl. Instrum. Methods Phys. Res., Sect. A **907**, 132 (2018).

[12]F. Bencivenga, R. Mincigrucci, F. Capotondi, L. Foglia, D. Naumenko, A. A. Maznev, E. Pedersoli, A. Simoncig, F. Caporaletti, V. Chiloyan, R. Cucini, F. Dallari, R. A. Duncan, T. D. Frazer, G. Gaio, A. Gessini, L. Giannessi, S. Huberman, H. Kapteyn, J. Knobloch, G. Kurdi, N. Mahne, M. Manfredda, A. Martinelli, M. Murnane, E. Principi, L. Raimondi, S. Spampinati, C. Spezzani, M. Trovò, M. Zangrando, G. Chen, G. Monaco, K. A. Nelson, and C. Masciovecchio, "Nanoscale transient gratings excited and probed by extreme ultraviolet femtosecond pulses," Sci. Adv. **5**, eaaw5805 (2019).
[13]F. Capotondi, A. A. Maznev, F. Bencivenga, S. Bonetti, D. Engel, D. Fainozzi, D. Fausti, L. Foglia, C. Gutt, N. Jaouen, D. Ksenzov, C. Masciovecchio, K. A. Nelson, I. Nikolov, M. Pancaldi, E. Pedersoli, B. Pfau, L. Raimondi, F. Romanelli, R. Totani, and M. Trigo, "Time-domain extreme-ultraviolet diffuse scattering spectroscopy of nanoscale surface phonons," Phys. Rev. Lett. **135**, 266101 (2025).
[14]C. Thomsen, H. T. Grahn, H. J. Maris, and J. Tauc, "Surface generation and detection of phonons by picosecond light pulses," Phys. Rev. B **34**, 4129 (1986).
[15]A. A. Maznev, "Boundary scattering of phonons: Specularity of a randomly rough surface in the small-perturbation limit," Phys. Rev. B **91**, 134306 (2015).
[16]S. V. Biryukov, Y. V. Gulyaev, V. V. Krylov, and V. P. Plessky, *Surface Acoustic Waves in Inhomogeneous Media*, Springer Series on Wave Phenomena Vol. 20 (Springer, 1995).
[17]J. Bonse, S. Höhm, S. V. Kirner, A. Rosenfeld, and J. Krüger, "Laser-induced periodic surface structures—A scientific evergreen," IEEE J. Sel. Top. Quantum Electron. **23**, 9000615 (2017).
[18]F. Capotondi, E. Pedersoli, N. Mahne, R. H. Menk, G. Passos, L. Raimondi, C. Svetina, G. Sandrin, M. Zangrando, M. Kiskinova, S. Bajt, M. Barthelmess, H. Fleckenstein, H. N. Chapman, J. Schulz, J. Bach, R. Frömter, S. Schleitzer, L. Müller, C. Gutt, and G. Grübel, "Invited article: Coherent imaging using seeded free-electron laser pulses with variable polarization: First results and research opportunities," Rev. Sci. Instrum. **84**, 051301 (2013).
[19]E. Allaria, L. Badano, S. Bassanese, F. Capotondi, D. Castronovo, P. Cinquegrana, M. Danailov, G. D'auria, A. Demidovich, R. De Monte *et al.*, "The FERMI free-electron lasers," J. Synchrotron Rad. **22**, 485 (2015).
[20]B. A. Auld, *Acoustic Fields and Waves in Solids* (Wiley, 1973), Vol. 1.
[21]J. P. Jones, "Wave propagation in a two-layered medium," J. Appl. Mech. **31**, 213 (1964).
[22]B. Auld, *Acoustic Fields and Waves in Solids* (John Wiley & Sons, 1973), Vol. 2.
[23]E. S. Fisher and C. J. Renken, "Single-crystal elastic moduli and the hcp → bcc transformation in Ti, Zr, and Hf," Phys. Rev. **135**, A482 (1964).
[24]E. B. Zaretsky, "Impact response of titanium from the ambient temperature to 1000 °C," J. Appl. Phys. **104**, 123505 (2008).
[25]W. A. Fate, "High-temperature elastic moduli of polycrystalline silicon nitride," J. Appl. Phys. **46**, 2375 (1975).
[26]W. Holmes, J. M. Gildemeister, P. L. Richards, and V. Kotsubo, "Measurements of thermal transport in low stress silicon nitride films," Appl. Phys. Lett. **72**, 2250 (1998).
[27]K. Singh, Y. Matsuda, K. Hattori, H. Nakano, and S. Nagai, "Non-contact sound velocities and attenuation measurements of several ceramics at elevated temperatures," Ultrasonics **41**, 9–14 (2003).
[28]I. A. Viktorov, *Rayleigh and Lamb Waves: Physical Theory and Applications* (Plenum Press, 1967).
[29]M. Schubert, M. Grossmann, C. He, D. Brick, P. Scheel, O. Ristow, V. Gusev, and T. Dekorsy, "Generation and detection of gigahertz acoustic oscillations in thin membranes," Ultrasonics **56**, 109 (2015).
[30]Z. Schaffer, P. Simeoni, and G. Piazza, "33 GHz overmoded bulk acoustic resonator," IEEE Microwave Wireless Compon. Lett. **32**, 656 (2022).
[31]M. Foerster, F. Macià, N. Statuto, S. Finizio, A. Hernández-Mínguez, S. Lendínez, P. V. Santos, J. Fontcuberta, J. M. Hernàndez, M. Kläui, and L. Aballe, "Direct imaging of delayed magneto-dynamic modes induced by surface acoustic waves," Nat. Commun. **8**, 407 (2017).
[32]N. K. P. Babu, A. Trzaskowska, P. Graczyk, G. Centała, S. Mieszczak, H. Głowiński, M. Zdunek, S. Mielcarek, and J. W. Kłos, "The interaction between surface acoustic waves and spin waves: The role of anisotropy and spatial profiles of the modes," Nano Lett. **21**, 946 (2021).
[33]J. Y. Lim, C. K. Ong, Y. Yao, and G. Chai, "Nonreciprocal interaction between Lamb waves, shear horizontal waves and spin waves at confined ferromagnetic heterojunction," J. Magn. Magn. Mater. **628**, 173120 (2025).